Desalination and Water Treatment
www.deswater.com

(2022) 238–248

doi: 10.5004/dwt.2022.28728

Application of improved multi-coupling model based on LH-OAT method in water environment simulation

Jianbo Pan[a], Wenjuan Zhang[b], Zhihui Liu[c], Xinping Shi[c], Zhanrui Chen[c,*]

[a]*School of Water Conservancy, North China University of Water Resources and Electric Power, Zhengzhou 450046, China*
[b]*Liaoyuan City Longshan District Agriculture and Forestry Work Station, Liaoyuan 136200, China*
[c]*Huizhou Hydroelectric Construction Engineering Co., Ltd., Huizhou 516003, China, email: czrhzsw@163.com (Z. Chen)*

Received 8 November 2021; Accepted 18 July 2022

ABSTRACT

Throughout this study, the LH-OAT method has been employed to optimize the parameters of the multi-coupling model, together with the improved multi-coupling model, to predict the pollution load scale of the Luxi River Basin in planning year. The conclusion is as follows: Applying the output of HEC-RAS coupling SWAT model, the loosely integrated multi-coupling model established can thoroughly simulate the water cycle in the basin. The average error between the calculated and the measured values of Yujiantan section flow, NH_3–N concentration, and TP concentration is respectively 7.00%, 13.85%, and 20.50%. In planning year, the forecast data of inflow pollution load in Luxi River basin demonstrates that the pollution load of NH_3–N point source into the river is 5,310.8 t/a, and that of non-point source into the river is 645.7 t/a, totaling 5,956.5 t/a; The corresponding data for TP is 531.1 and 89.1 t/a, totaling 620.2 t/a. The predicted spatial distribution of NH_3–N and TP non-point sources can afford solid support for water environment management in the basin.

Keywords: Multi-coupling model; LH-OAT method; Water environment; Prediction

1. Introduction

In the context of economic progress, the ecological environment of water bodies has been severely damaged [1]. According to the method pollutants enter the water body, pollution sources can be divided into point source pollution and non-point source pollution [2–4]. Point source pollution originates from definite places such as factories and sewage treatment plants whereas the origins of the non-point source pollution are quite scattered. Consequently, it is of paramount importance to conduct research on non-point source pollution. The SWAT (Soil Water Assessment Tools) model has been widely employed in simulating non-point source pollution in watersheds. It can not only be applied to large watersheds on a macro scale, but also present effective applicability in small watersheds [5]. Some scholars have availed themselves of the SWAT model to simulate the primary processes and pathways of nutrient migration in the Upper North Bosque River Basin, and have scored satisfying achievements [6]. Additionally, there are some scholars who have used the SWAT model to simulate the runoff and nutrients output in the Danube River Basin at different time and space scales as well as the runoff [7], sediment and pollutants in the Big Sunflower River Basin [8], and the controlling effects of different agricultural management measures on non-point source pollution of Heihe reservoir [9]. The application of SWAT model into these cases has witnessed effective simulation results, indicating that the model is suitable for watersheds in various climatic environments.

With significant strides in scientific and technological development, the simulation technology of river water quality has gradually become an important means of studying the transformation of pollutants and managing

* Corresponding author.

water environment pollution. The advance of water quality model is generally divided into three stages (Table 1) [10]. Hydrologic Engineering Center River Analysis System (HEC-RAS) is a common hydraulic analysis model, which can be used for one-dimensional constant flow, unsteady flow, sediment transport, water quality analysis and simulation etc. [11]. Since the hydrodynamic simulation mechanism is analogous to the MIKE 11 model, the former is often compared with the latter in terms of hydraulic calculations. Studies have shown that the results of the two are similar and both can achieve ideal simulation effects [12,13]. The HEC-RAS model has also been applied in the simulation of sediments and the results gained are relatively satisfactory [14,15]. In contrast, the research on employing HEC-RAS in water quality simulation is limited.

At present, the basin non-point source model has already exerted positive effects on the simulation of the pollution source load of the basin, and the hydrodynamic water quality model also has a mature system, yet both have their own shortcomings. The former cannot specifically describe the evolution process of pollutants after entering the water body, and the latter is difficult to obtain accurate input of non-point source pollution. As the water environment problems in river basins escalate, it is necessary to shift from a single water environment study to a coupling study of non-point source model and hydrodynamic water quality model. Some scholars have established the LWWM model by coupling the SWMM model and the WASP model and applied it to Lake Thonotosassa watershed and Kingston Harbour watershed [16–18]. Some experts have also adopted the method of coupling SWAT and QUAL2E to construct a multi-coupled model of water environment simulation system for the West Tiaoxi Watershed [19]. With the aid of LH-OAT (Latin Hypercube – One Factor at a Tim) method, this study optimizes the parameters of the multi-coupling model to ensure that it can effectively simulate the water quality and water volume changes in the basin. On the one hand, the research results can accomplish the comprehensive simulation of the basin water cycle. On the other hand, they can provide effective support for managing the basin water environment.

2. Materials and methods

2.1. Study area

Located on the southeastern edge of the Chengdu Plain (Fig. 1), the Luxi River Basin is higher in the northeast and lower in the southwest in terms of the overall terrain. Rested in an altitude of 1,000 m, the source of the river is a shallow cut hill with a landscape of structural denudation and erosion accumulation. The runoff of the basin mainly comes from precipitation. The fundamental parts of the feather-shaped watershed are on the southeast side of the main

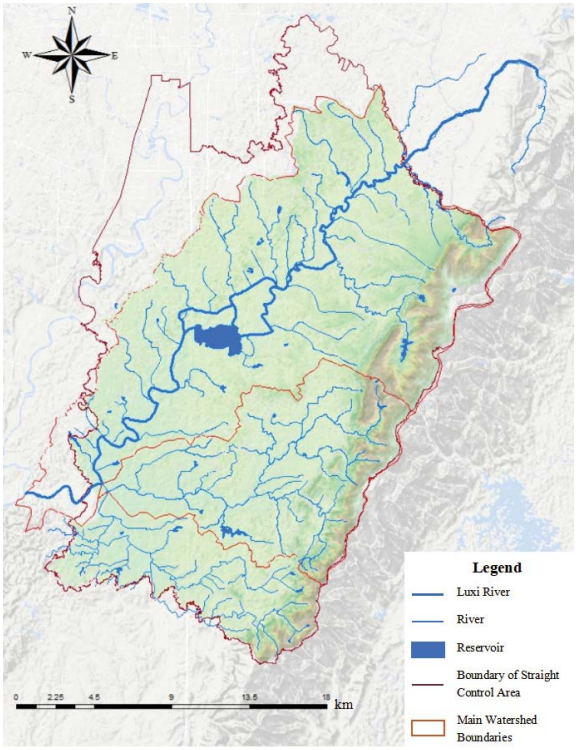

Fig. 1. Water system map of Luxi River Basin.

Table 1
Three stages of water quality model development

Stage of development	Typical model	Application water	Model characteristics
First-stage (1925s–2060s)	S-P model	Rivers	Model is relatively simple, a one-dimensional steady-state water quality model, and the simulated pollutants are relatively simple.
Second-stage (1960s–2080s)	QUAL Model System	Rivers	Model with increased complexity is suitable for studying the influence of multiple pollution components and pollution loads.
Third-stage (1980s–present)	MIKE, WASP, Delft, EFDC Model System	Rivers, lakes and reservoirs, estuaries, coastal waters	Model can be used for one-dimensional, two-dimensional, and three-dimensional calculations, and can be used for point source and area source analysis at the same time. It has independent sub-modules and can be combined with other models, but requires a lot of data as support, which is closer to the actual situation.

stream and the northwest side is the shallow hilly area in the eastern part of the Chengdu Plain (commonly known as the Dongshan hilly area). Luxi River is a first-level tributary of Jinjiang River and a second-level tributary of the Minjiang River, with a total length of 74.6 km, a drainage area of 675 km^2, and an average drop of 1.2‰. The maximum flood flow is 1,340 m^3/s, the low flow is only 0.02 m^3/s, and the multi-year average flow is 5.72 m^3/s. The average annual runoff for many years is 62 million m^3.

2.2. Construction of multi-coupling model

2.2.1. Construction of governing equations

The control equation of unsteady flow adopts one-dimensional Saint-Venant equations, where Eq. (1) is a continuous equation, and Eq. (2) is a momentum equation. The calculation equation is as follows:

$$\frac{\partial Q}{\partial x} + B\frac{\partial Z}{\partial t} = q \tag{1}$$

$$\frac{\partial Q}{\partial t} + \frac{\partial}{\partial x}\left(\frac{\alpha Q^2}{A}\right) + gA\frac{\partial Z}{\partial x} + g\frac{|Q|Q}{c^2 AR} = 0 \tag{2}$$

where t, time (s); x, distance (m); Q, flow (m^3/s); Z, water level (m); C, Xie Cai coefficient; A, cross-sectional area (m^2); B, water surface width (m); R, hydraulic radius (m); q, side flow rate per unit length (m^2/s); α, section unevenness coefficient.

The water quality control equation adopts a one-dimensional convection-diffusion equation:

$$\frac{\partial(AC)}{\partial t} + \left(\frac{\partial(QC)}{\partial x}\right) = \frac{\partial}{\partial x}\left(AE_x\frac{\partial C}{\partial x}\right) + A\frac{dC}{dt} + S \tag{3}$$

where A is the cross-sectional area of the water, m^2; C is the average centration of pollutants in the cross-section, mg/L; t is the time coordinate; Q is the average flow of the cross-section, m^3/s; x is the spatial coordinate; E_xE_xs the turbulent diffusion coefficient; dC/dt is the biochemical reaction term; S is the emission of pollutants, mg.

Table 2
Proportion of land use

Category of land use	Proportion of watershed
Farmland	68.04%
Forest	14.25%
Grassland	0.61%
Bush	0.003%
Wetland	0.02%
Water	1.29%
Impervious surface	15.70%
Bare land	0.09%
Farmland	68.04%

2.3. Construction of the database

The land use data selects the global land cover product FROM-GLC10 with 10-m resolution. The data covers a multi-season sample with uniform coverage of the world acquired from the interpretation of Landsat 8 images in 2014 and 2015 by experts. The land use data in the study area is divided into 8 categories, and the proportions of various types of land use are shown in Table 2.

The soil data is selected from the Harmonized World Soil Database version 1.1 (HWSD) constructed by the Food and Agriculture Organization of the United Nations (FAO) and the Vienna International Institute of Applied Systems (IIASA). The data originates from the 1:1 million soil data provided by the Nanjing Soil Institute of the Second National Land Survey. Meteorological data is presented by four consecutive monitoring days from 2013 to 2016, and the missing parts are estimated from nearby meteorological stations. Table 3 for point source pollution input through the survey of sewage discharge, and non-point source pollution through consulting the "Chengdu Statistical Yearbook" and surveying the statistics of agricultural fertilization management in the research area.

2.4. Discrete multi-coupling model

2.4.1. Scattering of research area

With the assistance of the GIS function, the model divides the basin into several sub-basins for simulation. The description parts of the basin are primarily to generate water systems, divide sub-basins, and add nodes such as point pollution sources, reservoirs, and water diversion from external basins. Input the DEM data and the digital river network into the model and define different minimum river catchment thresholds respectively then different numbers of sub-basins based on DEM will be generated. Grounded on the river network generated according to the results, comparison can be made with the actual river system. When determining the river network system, a threshold value of the minimum water catchment area of a river channel must first be given, which refers to the area necessary to form a permanent river channel. Units with upstream catchment area exceeding the threshold of the catchment area are defined as river courses, and less than this value is impossible to generate enough runoff to form a water course. The catchment area threshold can be changed. The smaller it is, the more detailed the net generated will be. However, if the threshold is too small, the generated river network will be too dense, resulting in pseudo river channels. Through trial and error method, 1,190 ha is finally selected as the minimum river catchment area threshold. Under this threshold, the generated river is more reasonable. Eventually, the entire study area is divided into 26 sub-basins, a total of 475.3 km^2. The average slope of each sub-basin is 9.22%, and the division numbers of specific sub-basin are shown in Fig. 2.

2.4.2. Discrete flow control equation

The quality of the differentiating format directly affects the accuracy and speed of the calculation results. Currently,

Table 3
Sewage discharge from sewage treatment plants

Serial	Name of the treatment plants	Actual processing capacity ten thousand/t/d	Emission standard	Water bodies discharged
1	Xinxing Liangshui Village sewage treatment plant	0.05	Level B Standard	Luxi River
2	Sewage treatment plant and off-site lifting pump station in Miaoshan Village, Xinxing Town	0.06	Level B Standard	Luxi River
3	Yongxingchang Town sewage treatment plant	0.06	Level B Standard	TiaoDeng River
4	Jitianchang Town sewage treatment plant	0.045	Level B Standard	Luxi River
5	Taipingchang Town sewage treatment plant	0.031	Level B Standard	Luxi River
6	Sanxingchang Town sewage treatment plant	0.04	Level B Standard	Chishui River
7	Sanxing Town agricultural products processing base sewage treatment station	0.114	Level B Standard	Chishui River
8	Baishachang Town sewage treatment plant	0.026	Level B Standard	Luxi River
9	Dalinchang Town sewage treatment plant	0.016	Level B Standard	Dongfengqu
10	Dalin Shimiao Village sewage treatment plant	0.018	Level B Standard	Dongfengqu
11	Xinglong Town sewage treatment plant	0.043	Level A Standard	Luxi River
12	Sencha Town sewage treatment plant	0.033	Level B Standard	Luxi River

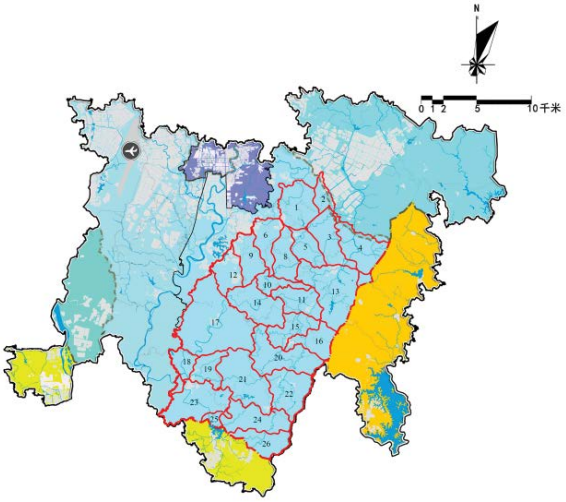

Fig. 2. Numbers of sub-basin.

there are various numerical calculation methods to afford solutions. Acclimating to different water flows and boundary conditions, these methods have their own merits and demerits. As far as the complexity of channel morphology and hydraulic characteristics of the reservoirs in the Luxi River basin is concerned, the Preissmann four-point implicit difference scheme with better stability is adopted here, and the discrete scheme is shown in Fig. 3.

The Preissmann four-point implicit difference scheme is shown:

$$\frac{\partial \xi}{\partial t} = \frac{\xi_i^{n+1} + \xi_{i+1}^{n+1} - \xi_i^n - \xi_{i+1}^n}{2\Delta t} \tag{4}$$

$$\frac{\partial \xi}{\partial x} = \frac{\theta\left(\xi_i^{n+1} - \xi_i^{n+1}\right) + \left(1-\theta\right)\left(\xi_{i+1}^n - \xi_i^n\right)}{\Delta x} \tag{5}$$

$$\xi = \frac{1}{2}\left(\xi_i^n + \xi_{i+1}^n\right) = \xi_{i+1/2}^n \tag{6}$$

where ξ is a variable, representing flow, water level, flow velocity, and river width etc., θ is a weight coefficient ($0 \le \theta \le 1$), when $\theta = 0$, this format is a display format, and when θ, this format has the feature of implicit difference. In order to keep the difference equation unconditionally stable, $\theta \ge 0.5$ must be guaranteed. The value of θ in this model is 0.75.

Substituting Eqs. (4) and (5) into the continuity equation and momentum equation respectively and sorting out, we get:

$$\begin{cases} -Q_i + C_i Z_i + Q_{i+1} + C_{i+1} Z_{i+1} = D_i \\ E_i Q_i - F_i Z_i + G_i Q_{i+1} + F_i Z_{i+1} = \varphi_i \end{cases} \tag{7}$$

The superscript at the end of the period $n + 1$ in the equations is omitted, and the coefficients in the equations are:

$$C_i = B_{i+1/2} \frac{\Delta x_i}{2\theta \Delta t} \tag{8}$$

$$D_i = -\frac{1-\theta}{\theta}\left(Q_{i+1}^n - Q_i^n\right) + C_i\left(Z_i^n + Z_{i+1}^n\right) + q_{i+1/2}\frac{\Delta x}{\theta} \tag{9}$$

$$E_i = \frac{\Delta x_i}{2\theta \Delta t} - (\alpha u)_i^n + \frac{g \Delta x_i}{2\theta}\left(\frac{|u|}{c^2 R}\right)_i^n \tag{10}$$

$$F_i = (gA)_{i+1/2}^n \tag{11}$$

$$G_i = \frac{\Delta x_i}{2\theta \Delta t} + (\alpha u)_{i+1}^n + \frac{g \Delta x_i}{2\theta}\left(\frac{|u|}{c^2 R}\right)_{i+1}^n \tag{12}$$

$$\varphi_i = \frac{\Delta x_i}{\theta \Delta t}\left(Q_{i+1}^n + Q_i^n\right) - \frac{(1-\theta)}{\theta}\left[(\alpha u Q)_{j+1}^n - (\alpha u Q)_j^n\right] - \frac{1-\theta}{\theta}(gA)_{i+1/2}^n\left(Z_{i+1}^n - Z_i^n\right) \tag{13}$$

where the subscript is $i + 1/2$, it means taking the average of the function values at the i and $i + 1$ sections. Since these six coefficients can be calculated according to the initial known value of the time period and the selected time step and distance step, the equations can be used to solve the water level and flow of each section.

2.4.3. Discrete water quality equation

The basic Eq. (3) is discretized with a staggered grid, and the discretization format adopts an implicit difference upwind style. The grid layout of the physical variables of the control equation and the distribution of the control volume are shown in Fig. 4.

The terms of the equation are discretized as:

$$\frac{\partial(AC)}{\partial t} = \frac{A_P^{n+1} C_i^{n+1} - A_P^n C_i^n}{\Delta t} \tag{14}$$

$$\frac{\partial(QC)}{\partial x} = \frac{\left(Q\bar{C}\right)_i^{n+1} - \left(Q\bar{C}\right)_{i-1}^{n+1}}{DX_P} \tag{15}$$

$$\frac{\partial}{\partial x}\left(AE_x \frac{\partial C}{\partial x}\right) = \frac{1}{DX_P}\left[\frac{(\text{AREA}_e)^{n+1}(E_x)_e^{n+1}}{0.5(DX_P + DX_E)}\left(C_{i+1}^{n+1} - C_i^{n+1}\right) - \frac{(\text{AREA}_w)^{n+1}(E_x)_w^{n+1}}{0.5(DX_P + DX_W)}\left(C_i^{n+1} - C_{i-1}^{n+1}\right)\right] \tag{16}$$

The superscript n is the initial value of the period, and the superscript n+1 is the end value of the period. In the following equations, the superscript is omitted for the end value of the period. When the convection term is discrete, the upside-down style is used:

$$\left(Q\bar{C}\right)_i = \frac{Q_i + |Q_i|}{2} C_i + \frac{Q_i - |Q_i|}{2} C_{i+1} \tag{17}$$

$$\left(Q\bar{C}\right)_{i-1} = \frac{Q_{i-1} + |Q_i|}{2} C_{i-1} + \frac{Q_{i-1} - |Q_{i-1}|}{2} C_i \tag{18}$$

Substituting Eqs. (14)–(18) into Eq. (3) and sorting out the following equations, we can obtain:

$$\alpha_i C_{i-1} + \beta_i C_i + \gamma_i C_{i+1} = \varphi_{i(i=L_1+1.....L2-1)} \tag{19}$$

In:

$$\alpha_i = -\frac{\Delta t}{DX_P}(\text{wa} + \text{wdif}) \tag{20}$$

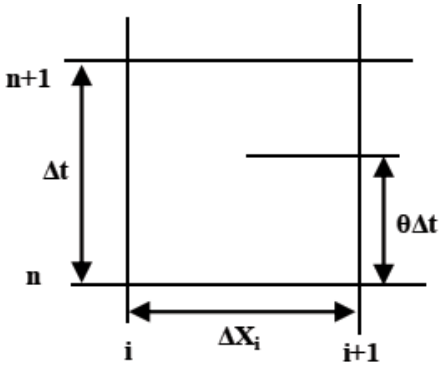

Fig. 3. The discrete scheme.

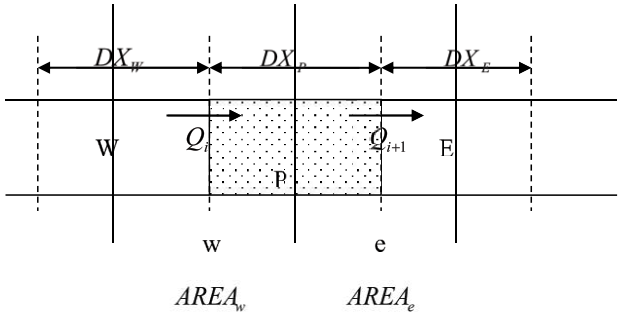

Fig. 4. Control volume of water quality equation.

$$\beta_i = A_P + \frac{\Delta t}{DX_P}\left(\text{ea} - \text{wd} + \text{edif} + \text{wdif}\right) + \Delta t \times K \times A_P \tag{21}$$

$$\gamma_i = \frac{\Delta t}{DX_P}\left(\text{ed} - \text{edif}\right) \tag{22}$$

$$\varphi_i = A_P^n C_i^n + \Delta t S_i \tag{23}$$

$$\text{ea} = \frac{Q_i + \left|Q_i\right|}{2} \tag{24}$$

$$\text{ed} = \frac{Q_i - \left|Q_i\right|}{2} \tag{25}$$

$$\text{wa} = \frac{Q_{i-1} + \left|Q_{i-1}\right|}{2} \tag{26}$$

$$\text{wd} = \frac{Q_{i-1} - \left|Q_{i-1}\right|}{2} \tag{27}$$

$$\text{edif} = \frac{\text{AREA}_e\left(E_x\right)_e}{0.5\left(DX_P + DX_E\right)} \tag{28}$$

$$\text{wdif} = \frac{\text{AREA}_w\left(E_x\right)_w}{0.5\left(DX_P + DX_w\right)} \tag{29}$$

Among them, L_1 and L_2 are the numbers of the first and last sections of the river. There are a total of L_2-L_1-1 equations above, plus two boundary conditions to form a three-diagonal matrix equation, and the concentration of each section can be calculated.

2.5. LH-OAT parameter modification

The LH-OAT method in this paper is a combination of the LH sampling method proposed by Mckay and the random OAT sensitivity analysis method put forward by Morris [20,21]. The basic idea of the LH sampling method is to divide the multi-dimensional parameters that meet the uniform distribution into N layers, and ensure each parameter is sampled only once and sampled N times, eventually randomly combined into N LH parameter groups. Although the LH sampling method with less frequency can guarantee the efficiency of sensitivity analysis, it is impossible to determine the change of which parameter has brought about that of the output value when all parameters are disturbed [22,23]. The essential concept of the OAT sensitivity analysis method is to analyze each parameter in the model by employing the controlled variable approach; namely when analyzing a certain parameter, it is assumed that other parameters remain constant and a certain disturbance is applied to the analyzed one. After running the model for several times, the sensitivity of each parameter can be obtained, but the swing amplitude of the output results is quite pertinent to the values of other parameters [24]. LH-OAT method, however, has not only done justice to their respective benefits but also avoids their shortcomings. It centers on obtaining several sets of data by stratifying each parameter in the analyzed ones and performing LH sampling to acquire a certain amount of data. With sensitivity analysis of each group of data, the sensitivity of each parameter in each group coupled with the average value of the sensitivity of each group of data can be known. This method can effectively identify the core parameter factors that exert effects on the model results, which significantly improves the credibility of the model parameters.

3. Results

3.1. Results of parameter sensitivity analysis

In this method, the model only analyzes the change of one parameter at a time with the others remaining unchanged. The parameters are sampled by stratification and randomly combined. Through multiple regression analysis, the operating results can clearly identify the parameters that lead to the changes. The results of sensitivity analysis of the parameters are shown in Table 4.

It can be observed from the sensitivity analysis that the core parameter affecting the area is SOL_K, followed by CANMX, mainly because the peak flow in summer is not obvious in the measured flow data, while in winter it is relatively apparent. Therefore, with a large flow of water replenishing the area, the base flow accounts for a relatively significant proportion, which has become the fundamental factors affecting the runoff process in this area.

3.2. Model calibration

3.2.1. Calibration of SWAT model

The calibration adjusts the initial, boundary conditions, model parameters and constraints to rendering the model close to the measured value. It is proven that the reliability of the model can be evaluated by verifying the independence of the residual series and the same variance test of the residual series. Two indicators, correlation coefficient (R^2) and Nash-Suttcliffe model efficiency coefficient E_{ns}() are selected to evaluate the simulation results. Calculated as follows:

(1) The certainty coefficient E_{ns} the overall comprehensive index displays the quality of the entire runoff simulation, generally between 0–1. The larger the value is, the more reliable the model's operation is. The general evaluation standard of simulation efficiency is E_{ns}.5:

$$E_{ns} = 1 - \frac{\sum_{i=1}^{n}\left(O_i - S_i\right)^2}{\sum_{i=1}^{n}\left(O_i - O\right)^2} \tag{30}$$

Table 4
Parameter sensitivity analysis results

Parameter name	Physical meaning	*t*-value	*P*-value
R__SOL_K.sol	Soil saturated hydraulic conductivity/mm h^{-1}	35.87	0.00
V__CANMX.hru	Maximum canopy interception	4.08	0
R__SOL_Z.sol	Depth of soil surface to bottom	2	0.05
V__CH_K2.rte	Effective hydraulic conductivity of the main river bed	–1.5	0.13
V__SURLAG.bsn	Surface runoff lag coefficient	–1.46	0.14
V__TIMP.bsn	Snow temperature lag coefficient	–1.26	0.2
V__RCHRG_DP.gw	Permeability ratio of deep aquifer	1.24	0.21
R__CN2.mgt	The initial SCS runoff curve under humid conditions is sparse	1.1	0.27
V__GW_DELAY.gw	Groundwater delay time/d	0.96	0.33
R__SOL_ALB.sol	Albedo of moist soil	–0.96	0.33
R__SOL_BD.sol	Saturated soil bulk density	0.95	0.34
V__SLSUBBSN.hru	Average slope length	0.79	0.42
V__EPCO.hru	Plant absorption compensation factor	0.78	0.43
R__BIOMIX.mgt	Biological mixing efficiency	–0.71	0.47
V__CH_N2.rte	Manning coefficient of main channel	–0.65	0.51
V__GW_REVAP.gw	Shallow groundwater re-evaporation coefficient	–0.51	0.6
V__OV_N.hru	Manning slope overflow n value	0.48	0.62
V__TLAPS.sub	Vertical temperature decline rate	–0.4	0.68
V__HRU_SLP.hru	Average slope	–0.3	0.76
R__SOL_AWC.sol	Effective water capacity of soil layer	0.26	0.79
V__ALPHA_BF.gw	Base flow alpha factor	0.24	0.8
V__GWQMN.gw	The threshold depth at which shallow aquifers produce "base flow"	–0.08	0.93
V__REVAPMN.gw	The threshold depth at which shallow aquifers "reevaporate" or penetrate into deep aquifers	0	0.99

The larger the absolute value of the *t*-value is, the more sensitive the parameter is; the *p*-value indicates the significance of the *t*-value, and the smaller the *p*; value is, the slimmer the chance that the parameter is accidentally designated as a sensitive parameter is.

where o_i s the measured value; S_i is the analog value; O is the average f the measured value; n is the number of samples.

(2) Linear fitting coefficient R^2 indicates the fitting degree between the simulated value and the measured value curve, taking the value 0–1. The larger the value is, the better the fitting effects are. Generally, $R^2 > 0.6$ is used as the evaluation standard of the simulated fitting degree:

$$R^2 = \left\{ \frac{\sum_{i=1}^{n}\left(O_i - O\right)\left(S_i - S\right)}{\left[\sum_{i=1}^{n}\left(O_i - O\right)^2\right]^{0.5}\left[\sum_{i=1}^{n}\left(S_i - S\right)^2\right]^{0.5}} \right\}^2 \tag{31}$$

As there is no measured hydrological data in the Luxi River Basin and merely the monthly average flow data for 2015 and 2016 are available, this study selected the period from 2013 to 2016 for simulation, of which 2013–2014 is the warm-up period of the model, 2015 the model rate regular, and 2016 the model verification period. Fig. 5 presents the fitting process of the flow in the simulated Yujiantan section.

The Nash-Suttcliffe coefficient $E_{ns}n$ the regular and verification period of Yujiantan is 0.75/0.51 and the correlation coefficient R^2 is 0.88/0.78, which satisfies the requirements of the model. The Nash–Suttcliffe coefficient $E_{ns}f$ the NH_3–N concentration rate is 0.64/0.63 and the correlation coefficient R^2 is 0.82/0.84 during the regular and verification period. The Nash–Suttcliffe coefficient $E_{ns}f$ TP concentration rate is 0.71/0.51 and the correlation coefficient R^2 is 0.91/0.72, fulfilling the requirements of the model.

3.2.2. Calibration of water quality equation

The water quality items simulated by the equation include NH_3–N and TP. For different water quality projects, the biochemical reaction term dc/dt in the equation differs. Under the constraints of existing data and other factors, the following first-order reaction kinetic equations are applied to describe the biochemical reaction items according to the actual situation.

(1) Ammonia nitrogen (CNH):

$$\frac{dC_{\mathrm{NH}}}{dt} = \frac{\sigma_{\mathrm{NH}}}{A} J_{\mathrm{NH}} C_{\mathrm{NH}} \tag{32}$$

where σ_{NH} is the rate at which nitrogen is released from the bottom sludge, unit: 1/s; J_{NH} is the denitrification rate constant, unit: 1/s;

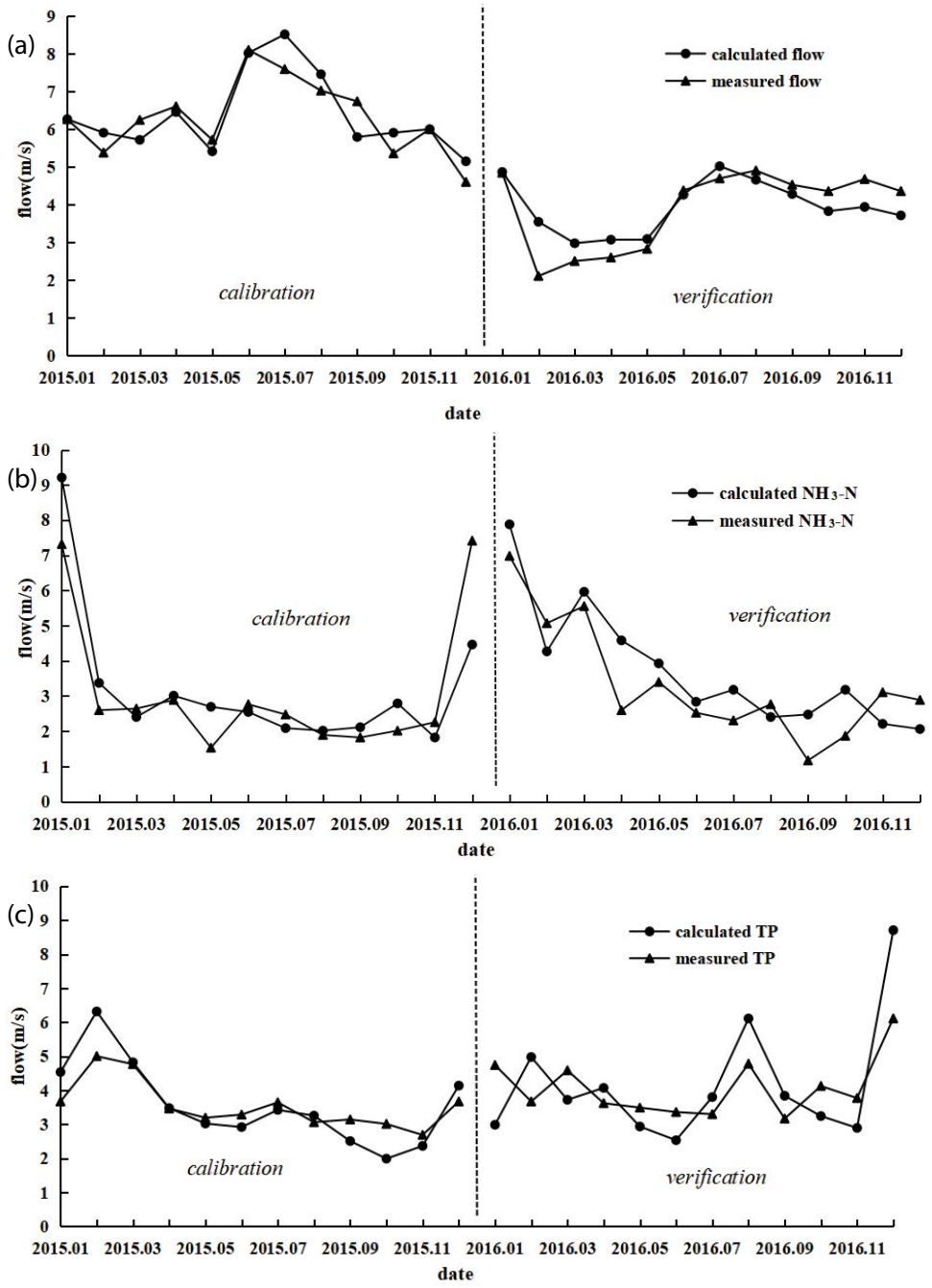

Fig. 5. (a) Flow process in regular and verification period of Yujiantan. (b) Comparison chart of NH_3–N process in regular and verification period of Yujiantan. (c) Comparison chart of the TP process in regular and verification period of Yujiantan.

(2) Total phosphorus TP (C_p):

$$\frac{dC_p}{dt} = \frac{\sigma_p}{A} J_p C_p \tag{33}$$

In the equation: σ_p is the rate of phosphorus released from the sediment, unit: 1/s; J_p is the rate of phosphorus sedimentation, unit: 1/s.

The model is calibrated based on the current water quality and water quantity data of the Yujiantan section in Luxi River in 2015. The results are presented in Fig. 6 and Table 5. It can be known that the results of flow and water quality simulated by the model are basically approaching the measured values. The average relative error between the measured fl and the calculated flow of the model is 7.00%, and the corresponding data for NH_3–N concentration and TP is respectively 13.85% and 20.50%, demonstrating

Table 5
The prediction error of the measured and calculated values of Yujiantan section

Month	Measured values			Calculated values			Relative error (%)			Average relative error (%)		
	Flow (m^3/s)	NH_3–N concentration (mg/L)	TP concentration (mg/L)	Flow (m^3/s)	NH_3–N concentration (mg/L)	TP concentration (mg/L)	Flow	NH_3–N concentration	TP concentration	Flow	NH_3–N concentration	TP concentration
1	23.6	5.68	0.67	22.7	6.09	0.87	3.96	6.72	22.74	7.00	13.85	20.50
2	19.7	2.90	0.89	20.53	3.73	1.17	4.04	22.17	24.00			
3	23.5	1.63	0.26	20.67	2.12	0.32	13.69	22.99	17.58			
4	25.3	7.30	0.43	23.84	9.34	0.53	6.12	21.83	18.99			
5	21.1	1.30	0.36	19.11	1.65	0.29	10.41	21.28	23.28			
6	32.1	1.63	0.39	30.3	1.66	0.40	5.94	1.60	3.52			
7	30.1	1.36	0.41	29.36	1.25	0.33	2.52	9.14	24.52			
8	27.1	0.79	0.35	28.89	0.80	0.28	6.20	1.24	23.99			
9	25.8	0.84	0.31	22.29	0.87	0.25	15.75	3.86	23.08			
10	19.7	1.53	0.34	20.9	2.02	0.29	5.74	24.22	19.13			
11	22.4	1.09	0.29	21.96	0.97	0.24	2.00	12.57	21.35			
12	16.2	5.68	0.49	17.49	6.97	0.64	7.38	18.52	23.83			

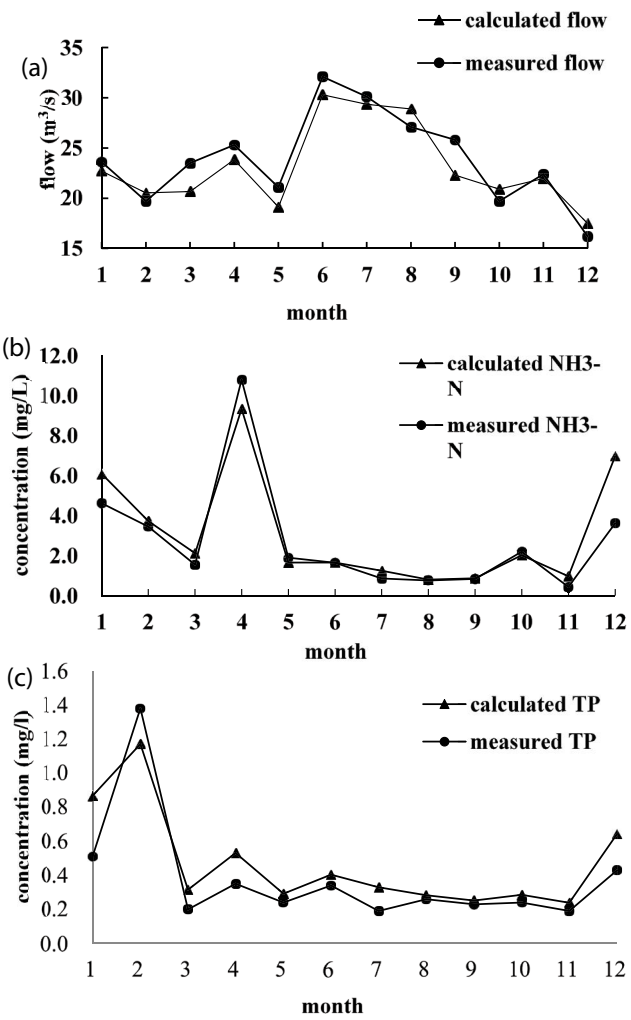

Fig. 6. (a) Comparison of measured and calculated values of flow at Yujiantan section. (b) Comparison of measured and calculated values of NH_3–N at Yujiantan section. (c) Comparison of measured and calculated values of TP at Yujiantan section.

that the established hydrodynamic water quality model can largely simulate the change law of the water volume and water quality of the Luxi River in an accurate manner, and can be adopted for simulation and prediction calculations.

3.3. Prediction of annual pollutants into the river

Taking 30 y from the current year as the planning year, the average influent water quality of the sewage treatment plants in the Luxi River Basin is 200 mg/L COD, 30 mg/L NH_3–N, and 3 mg/L TP based on investigation. According to the survey results and the data of the Environmental Protection Agency, the per capita sewage discharge coefficient of rural domestic sources in the basin is estimated to be 238.8 L/person·d, and the comprehensive pollution production coefficients of COD, NH_3–N and TP are respectively 79, 8.7 and 5.5 g/d. In the livestock and poultry breeding industry, 30 laying hens are converted into 1 pig, 60 broilers

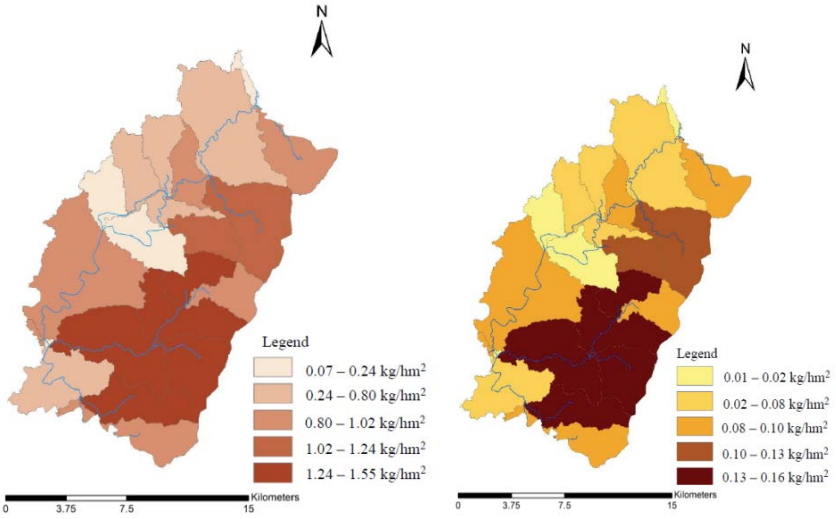

Fig. 7. NH_3–N non-point (a) and TP non-point (b) source distribution in planning year.

Table 6
The pollution load scale of the Luxi River Basin in planning year (unit: t/a)

Point and non-point source	Types of pollution source	NH_3–N (t/a)	TP (t/a)
Point source	Town life and industry	5,310.8	531.1
Non-point source	Rural life	323.9	84.3
	Free-range livestock and poultry	127.6	2.6
	Farmland runoff	194.2	2.2
	Subtotal	645.7	89.1
Total		5,956.5	620.2

into 1 pig, 1 cow into 10 pigs, 1 cattle into 5 pigs. Take the pollution discharge coefficient of the pig as COD 47.09 g/head·d, total nitrogen 5.56 g/head·d, TP 0.43 g/head·d, and the coefficient of farmland runoff source intensity COD 10 kg/mu·a, NH_3–N 2 kg/mu·a, and TP 0.055 kg/mu·a. In the planning year, the estimated pollutant inflow into the Luxi River Basin is shown in Table 6, and the distribution of ammonia nitrogen-grade phosphorus source is displayed in Fig. 7.

From the perspective of the types of pollution sources, the urban population has reached 1.5 million, and the amount of pollution generated has also increased correspondingly. The rural population is about 150,000, and the amount of non-point source pollution in rural life remains to be relatively prominent. Non-point source pollution from farmland runoff maintains to be an indispensable source of pollutants. In the light of the distribution area of pollution sources, the origins are concentrated in the southeast and the runner-up is the southwest. As a result of the population in the southeast region increased to 400,000 during the planning year, among which the rise in the industrial compatibility communities takes up the largest percentage, new pollution loads have been inflicted upon the region. Even though scarce changes have taken place in the majority of the farmlands of the southwest, more farmland non-point source pollution is still produced.

4. Conclusion

In this paper, ArcSWAT is employed to establish a non-point source model in the Luxi River Basin to simulate the hydrology and pollutant transport process in the watershed. With the aid of the HEC-RAS coupling SWAT model output, the water environment simulation system of the watershed multi-coupling model is constructed, which is a loosely integrated coupling model and makes it to simulate the whole process of the basin water cycle. This paper adopts the LH-OAT method for sensitivity analysis and calibration verification of model parameters, ensuring both the prominence of the sensitivity of a single parameter and the correlation among parameters. Suitable for the sensitivity analysis of multi-coupling model parameters, this method significantly reduces the workload while improving the accuracy.

According to the actual situation, the monitoring data of water quality and water volume in the Yujiantan section are used to verify the flow rate, NH_3–N concentration, and TP concentration. The results indicate that the regular rate and the Nash–Suttcliffe coefficient during the verification period satisfies the requirements of the model. The average error between the calculated and measured values of Yujiantan section flow is 7.00%, and the corresponding data for NH_3–N concentration and TP concentration is respectively 13.85% and 20.50%.

By predicting the emission coefficients of various pollution sources and resorting to an improved multi-coupling model, the pollution load scale of the Luxi River Basin in planning year can be anticipated: the pollution load of NH_3–N point source into the river is 5,310.8 t/a, non-point source into the river is 645.7 t/a, totaling 5,956.5 t/a; the pollution load of TP point source into the river is 531.1 t/a, and the pollution load of TP non-point source into the river is 89.1 t/a, totaling 620.2 t/a. The corresponding data for TP is 531.1 t/a and 89.1 t/a, totaling 620.2 t/a. The multi-coupling model presents sound applicability in basin water quality simulation, and can be employed to predict and analyze the migration law of NH_3–N and TP. The predicted spatial distribution of NH_3–N and TP non-point sources can afford solid support for water environment management in the basin.

References

[1] H. Chansheng, F. Bojie, C. Liding, Management and control of non-point source pollution, Environ. Sci., 5 (1998) 88–92, 97 (in Chinese).

[2] O. Wei, L. Yingchun, L. Siwen, L. Hongbin, W. Yidi, Analysis on the development trend of non-point source pollution research in recent 30 years, J. Agro-Environ. Sci., 37 (2018) 150–157 (in Chinese).

[3] Y. Xuhua, Z. Liang, C. Lin, W. Xinming, F. Changfeng, Z. Yuehua, Q. Yunpeng, T. Xiangjun, Application of ArcGIS in spatial analysis of water source pollution intensity, J. Hohai Univ. (Nat. Sci. Ed.), 46 (2018) 23–29 (in Chinese).

[4] H. Gairui, L. Jiake, L. Huaien, L. Kangbin, Y. Liu, Research progress of non-point source pollution models and uncertainty analysis methods in watershed, J. Hydroelectric Eng., 12 (2018) 54–64 (in Chinese).

[5] J.G. Arnold, J.R. Williams, A.D. Nicks, N.B. Sammons, SWRRB; A Basin Scale Simulation Model for Soil and Water Resources Management, Texas A & M University Press, College Station, Texas, 1990.

[6] A. Saleh, J.G. Arnold, P.W. Gassman, L.M. Hauck, W.D. Rosenthal, J.R. Williams, A.M.S. McFarland, Application of SWAT for the upper North Bosque River watershed, Trans. ASAE, 43 (2000) 1077–1087.

[7] M.K. Shrestha, F. Recknagel, J. Frizenschaf, W. Meyer, Assessing SWAT models based on single and multi-site calibration for the simulation of flow and nutrient loads in the semi-arid Onkaparinga catchment in South Australia, Agric. Water Manage., 175 (2016) 61–71.

[8] A.O. Dakhlalla, P.B. Parajuli, Assessing model parameters sensitivity and uncertainty of streamflow, sediment, and nutrient transport using SWAT, Inf. Process. Agric., 6 (2019) 61–72.

[9] L. Wang, Research on Non-point Source Pollution of Heihe Reservoir Based on SWAT Model, Xi'an University of Technology, China, 2015 (in Chinese).

[10] L. Shasha, S. Lianqiang, Review on the development of water quality modeling, Environ. Eng., 34 (2016) 78–81 (in Chinese).

[11] M.S. Khattak, F. Anwar, T.U. Saeed, Floodplain mapping using HEC-RAS and Arc GIS: a case study of Kabul River, Arabian J. Sci. Eng., 4 (2016) 1375–1390.

[12] L. Li, Z. Yi, C. Yuxiang, Analysis of flood calculation results of MIKE 11 and HEC-RAS hydrodynamic model, Zhejiang Water Resour. Sci. Technol., 47 (2019) 17–20 (in Chinese).

[13] C. Xuedong, Q. Yong, Z. Weixia, K. Luzhi, L. Yunchun, Numerical simulation of mountain natural river surface based on HEC-RAS and MIKE 11, People's Pearl River, 35 (2014) 116–118 (in Chinese).

[14] I. Mondal, J. Bandyopadhyay, A.Kr. Paul, Estimation of hydrodynamic pattern change of Ichamati River using HEC RAS model, West Bengal, India, Model. Earth Syst. Environ., 2 (2016) 1–13.

[15] R. Kasperek, M. Mokwa, M.J. Wiatkowski, Modeling of pollution transport with sediment on the example of the Widawa River, Arch. Environ. Prot., 2 (2013) 29–43.

[16] T.A. Wool, J.L. Martin, R.W. Schottman, The linked watershed/waterbody model (LWWM): a watershed management modelling system, Lake Reservoir Manage., 9 (1994) 124.

[17] M. Kelly, R. Giovannelli, Linked Watershed/Water-Body Model, 1epa Seminar Publication, 1995, pp. 202–212.

[18] M.O. Walters, H. Thomas, Application of a Linked Watershed Water Body Model to Kingston Harbour in Jamaica, IAHS Publication (International Association of Hydrological Sciences), 1998, pp. 137–146.

[19] L. Dan, X. Lianqing, H. Zhenchun, Impact analysis of watershed non-point source pollution simulation based on SWAT model, Environ. Pollut. Control, 3 (2008) 4–7 (in Chinese).

[20] M.D. McKay, R.J. Beckman, W.J. Conover, A comparison of three methods for selecting values of input variables in the analysis of output from a computer code, Technometrics, 21 (1979) 239–245.

[21] M.D. Morris, Factorial sampling plans for preliminary computational experiments, Technometrics, 33 (1991) 161–174.

[22] Z. Jiaqi, X. Xiangyang, H. Shuang, Parameter sensitivity analysis of SWMM model based on LH-OAT, China Rural Water Hydropower, 3 (2014) 84–87 (in Chinese).

[23] X. Fang, Q. Wang, J.C. Wang, X.Y. Xiang, Y.F. Wu, Y.F. Zhnag, Employing extreme value theory to establish nutrient criteria in bay waters: a case study of Xiangshan Bay, J. Hydrol., 603 (2021) 127146, doi: 10.1016/j.jhydrol.2021.127146.

[24] L. Hui, J. Sheng, L. Xiaoyun, Z. Lianyong, Z. Xiang, Sensitivity analysis of SWAT model parameters and importance of automatic calibration Take runoff simulation of Manas River as an example, J. Water Resour. Water Eng., 21 (2010) 79–82 (in Chinese).